SPECIAL SECTION ON ADDRESSING CHALLENGING ISSUES OF GRIDS WITH HIGH PENETRATION OF GRID CONNECTED POWER CONVERTERS: TOWARDS FUTURE AND SMART GRIDS

IEEE Access
Multidisciplinary ⋮ Rapid Review ⋮ Open Access Journal

Received April 25, 2020, accepted May 20, 2020, date of publication June 2, 2020, date of current version June 12, 2020.

Digital Object Identifier 10.1109/ACCESS.2020.2999336

A Novel Application of Harmonics Spread Spectrum Technique for Acoustic Noise and Vibration Reduction of PMSM Drive

RAJESH M. PINDORIYA[1], (Graduate Student Member, IEEE), BHARAT SINGH RAJPUROHIT[1], (Senior Member, IEEE), AND RAJEEV KUMAR[2], (Senior Member, IEEE)

[1]School of Computing and Electrical Engineering, IIT Mandi, Mandi 175075, India
[2]School of Engineering, IIT Mandi, Mandi 175075, India

Corresponding author: Rajesh M. Pindoriya (rajeshpindoriya@ieee.org)

This work was supported by the Naval Research Board, India.

ABSTRACT This paper presents experimental investigation study of Acoustic Noise and Vibration (ANV) reduction in Permanent Magnet Synchronous Motor (PMSM) drives with a novel application of 'harmonics spread spectrum technique'. In order to reduce the ANV of PMSM drives, the Random Pulse Width Modulation (RPWM) method is applied which distributes the power of harmonic noise in a wide range of discrete frequency spectrum. Furthermore, in-depth theoretical analysis is presented about the way RPWM improves torque ripples, vibration and acoustic noise in PMSM drives. The theoretical and experimental results obtained are used to draw the operational concept of the power electronics converters to reduce ANV; which is produced by PMSM drive. Time and frequency-domain analysis are carried out to examine the effects of change in the operating parameters such as pulse-width, etc. of the power electronics converters on the ANV. A small-scale laboratory set-up was developed for PMSM drive with low cost acoustic chamber for experimental investigations. Experimental results show significant reduction in ANV and torque ripples of the PMSM drive with the application of RPWM technique.

INDEX TERMS Acoustic noise and vibration (ANV), harmonic spread spectrum technique, permanent magnet synchronous motor (PMSM) drive, random pulse width modulation (RPWM) technique and time-domain analysis.

I. INTRODUCTION

The Permanent Magnet Synchronous Motors (PMSM) are the most promising drives in the industries. Its numerous advantages, such as, high torque to power ratio, flexibility in operation and control, and high magnetic field density have made it widely used motor for many applications.

The alternating flux in the air-gap in a working machine is responsible for the efficient production of torque. In turn this flux results in fluctuating mechanical forces in the stator which give rise to a lot of Acoustic Noise and Vibration (ANV) in the frame of the motor and its surroundings [1]. The challenges related to ANV have attracted a numbers of power engineering researchers since last decade [2]–[5].

The associate editor coordinating the review of this manuscript and approving it for publication was Dinesh Kumar.

It has been reported, that the dominating source for vibration in the low- to medium-power rated machines is electromagnetic sources. The radial forces are the main electromagnetic sources of ANV in well-designed motors [5]. The spectrum of radial magnetic forces comprises many existing harmonic sources in the machines. The stator Magneto-Motive Force (MMF) harmonics are the most common. The frequency of radial electromagnetic force harmonics is a multiple of switching frequency [4]. In addition, the switching losses and adverse effects, caused by high dv/dt, are considerably large in heavy industrial and railway traction application drives. This causes unpleasant acoustic noise development in industrial applications, such as electric vehicles and elevators, which is needed researchers attentions. Therefore, the switching frequency of the power devices is severely restricted for their application in such drives [5].

Recent reported research work addresses the ANV and its possible reduction strategies [6]–[10]. Two major techniques are adopted to make the system noiseless, first; to improve the design of the machine and second; to adopt the innovative drive control strategies. Although considerable work has been done for the reduction of ANV through design innovations, however, still there is a scope for newer solutions through control techniques. Binojkumar *et al.* [4] in 2015 has presented the experimental results of acoustic noise investigations generated by induction motor at diverse frequencies and over a range of carrier frequencies.

Fang and Zhang [5] in 2018 presented parameters such as space harmonic and time harmonics responsible for the generation of ANV in electrical machines. Authors also performed an analysis of time harmonics on the three-phase voltage source inverter and mechanical gear system. This work uses the findings for the design the mechanical components and its aerodynamic structures, which is a function of the carrier frequency of the converters.

Motor designers have proposed to increase the shape of the flux barrier in rotor and stator teeth of the machine to decrease the ANV. Zhu and Jewell [6] in 2009 has presented a way to optimize the shape of the magnets and stator teeth in order to decrease the ANV. Yang *et al.* [7] in 2013 has presented ANV reduction of a single-phase switched reluctance motor using skewed stator and rotor. The fast-changing radial magnetic field in air-gap between stator and rotor poles is the main source of ANV. It is observed that the maximum intensification of the radial forces is on the stator yoke in proximity with salient poles. Hence the rapid change in the radial force can be reduced by making stator and rotor laminations skewed.

Jang *et al.* [8] in 2010 has presented the ways to reduce the ANV in interior PMSM type integrated starter and generator for a hybrid electric vehicle. This paper showed two major ways to reduce the ANV in the PMSM drive. One way is to enhance the stiffness of the stator yoke and another way is to decrease the prevailing electromagnetic forces. By reducing stator stiffness, the white noise has been reduced. However, a compromise with the increased size of the motor was needed to provide the noise solution. Hence, focus is needed on the reduction of existing electromagnetic forces.

Trzynadlowski *et al.* [9] in 1994 has summarized the responsibility and application of Random Pulse Width Modulation (RPWM) technique for a converter-fed induction motor drive system. The paper analyzed RPWM application for voltage-controlled power electronic converters for a beneficial impact on the ANV of electric drives. The idea behind random PWM modulation methods is that the power of harmonic noise is distributed in a wide range of discrete frequency spectrum. In simple words, randomization of the 'pulse width position' acuminates the spectrum by reducing most harmonics below the level of the continuous spectrum and leaving narrow clusters of harmonics in the close proximity of multiples of the power converter switching frequency [9].

The wide spread spectrum necessarily not to be considered a disadvantage of the randomization scheme as reported in Zhang *et al.* [10], since the central frequencies of the power converter switching frequency clusters, can be disciplined by adjusting the number of switching intervals [11].

The randomization of the switching patterns affects the noise in two ways. First, it reduces the susceptibility of the drive system to mechanical resonances, which in certain cases results in the decrease of the overall noise level. Second and predominantly, it changes the subjective perception of the noise, as the annoying tonal component becomes spread into a wideband atonal noise [9].

On similar lines, Basu *et al.* [12] in 2009 has presented various PWM topologies to reduce the current and torque ripple in three-phase inverter-fed induction motor drives. In [12], authors have experimentally validated the proposed approach to decrease the Root Mean Square (RMS) current and torque ripple by around 30% at the rated speed of the motor drive as compared to the conventional space vector PWM approach.

Pindoriya *et al.* [13] in 2019 has presented that how power electronic converters inject harmonics and produce electromagnetic forces that produce ANV in PMSM drive and furthermore noise is radiated from motor structure to its surrounding. Further authors presented the application of pseudorandom PWM technique i.e. one of the harmonic spread spectrum techniques for PMSM drives supported with simulation results. An extensive study of application of Random Pulse Width Modulation (RPWM) techniques, specifically 'random pulse position', for PMSM based drive for reduction of Acoustic Noise and Vibration (ANV) seems absent from the reported literature. Hence, in this present paper, a novel control approach based on random PWM technique i.e. random pulse position has been discussed and implemented experimentally to validate its effectiveness in order to reduce the ANV in PMSM drive. In random pulse position RPWM technique, the total time i.e. $T_{on} + T_{off}$ (or switching frequency) remains constant, however, pulse position is randomly varying. The relationships between the stator current harmonics/ripples feed by power electronics converters and non-sinusoidal magnetic field flux distribution, with torque harmonics/ripple is developed and analyzed in this paper. Furthermore, in-depth theoretical background about the way RPWM improves torque ripples, vibration and acoustic noise of PMSM drives is also presented.

A small-scale laboratory set-up is developed for PMSM drive with low cost acoustic chamber for experimental validation. Experimental and simulation results are obtained for acoustic noise, torque ripples and vibrations to validate the effectiveness of proposed RPWM technique.

The organization of this paper is as follows; Section-II present sources of ANV in PMSM. Section-III presents the theoretical background of RPWM technique and design of control loops of PMSM drive. Section-IV gives non-linear electrodynamic modelling of PMSM drive. Section-V presents the detailed simulation and experimental investigation of the PMSM drive for ANV reduction.

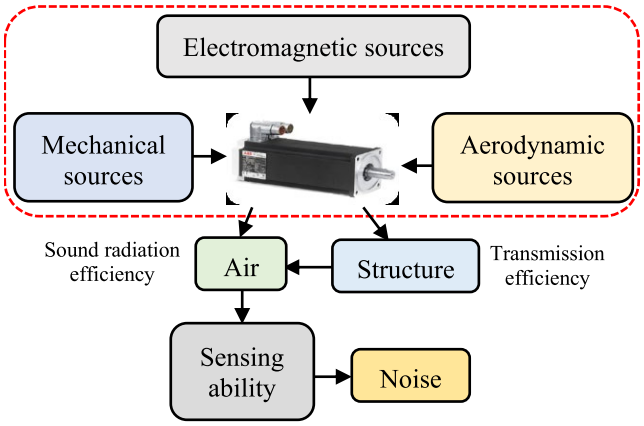

FIGURE 1. Pictorial representation of the generation of noise and its propagation in electrical machines.

II. SOURCES OF ACOUSTIC NOISE AND VIBRATION IN ELECTRIC DRIVES

For an electrical machine, the ANV has been classified in the following three categories, viz. aerodynamic, mechanical and electromagnetic source as shown in Fig. 1 [1]. For PMSM, the ANV is primarily produced by stator flux, not the rotor, as the rotor is made up of permanent magnets.

The converter-fed PMSM drive uses solid-state power electronic converters which supplies non-sinusoidal voltage source and in-turn non-sinusoidal currents to the drive system. PWM harmonics in stator currents which generates harmonics in stator MMF which in-turn contributes to radial magnetic forces causing vibration in the machine. Depending on systems configuration, the frequency of the generated harmonics may be lower or higher order. The harmonics of the order 3^{rd}, 5^{th}, 7^{th}, and 11^{th} are of significance since the higher-order harmonics are neglected due to low magnitudes. The ripples produced in the torque signals finally contribute to acoustic noise or EMI. Expression of electromagnetic torque T_{em} of converter-fed PMSM suitable to study the effects of non-sinusoidal current can be derived as follows [14]. A three-phase balanced PMSM has three-phase stator windings electrical phase-shifted in space by $120°$. The peak current in each phase is given by $\sqrt{2}\,I$ which is also phase-shifted by $120°$. The instantaneous currents in all three-phase windings are given as (1)-(3);

$$i_a(\mathrm{t}) = \sqrt{2}\,I\,cos\,(\omega t) \tag{1}$$

$$i_b(\mathrm{t}) = \sqrt{2}\,I\,cos\left(\omega t - \frac{2\pi}{3}\right) \tag{2}$$

$$i_c(\mathrm{t}) = \sqrt{2}I\,cos\left(\omega t - \frac{4\pi}{3}\right) \tag{3}$$

where, $i_a(t)$, $i_b(t)$ and $i_c(t)$ are instantaneous value of current of phase-a, phase-b and phase-c respectively. I is fundamental current of the PMSM drive and ω is angular frequency of rotor. At instant t, the instantaneous electromagnetic torque produced by phase-a winding of PMSM is the interaction of the magnetic field $B\,(\alpha, t)$ and the current $i_a(t)$ circulating in N conductors [14]:

$$T_a\,(t) = 2pN \int_{-\pi/6p}^{\pi/6p} RlB\,(\alpha, t)\,i_a\,(t)\,d\alpha \tag{4}$$

or

$$T_a\,(t) = i_a(t) \cdot \left[2pN \int_{-\pi/6p}^{\pi/6p} RlB\,(\alpha, t)\,i_a\,(t)\,d\alpha\right] \tag{5}$$

where, T_a is electromagnetic torque produced by phase-a, p is number of pole pairs, N is number of conductors, R is radius of stator core, l is active length of motor, B is magnetic field, and α is space angle.

The back-EMF induced in phase-a at instant t is given by

$$e_a\,(t) = 2pN \int_{-\pi/6p}^{\pi/6p} B\,(\alpha, t)\,lR\omega_m\,d\alpha \tag{6}$$

where ω_m is the rotor angular speed and e_a is back-EMF of phase-a. The EMF $e_a(t)$ can be written as

$$e_a\,(t) = \omega_m \left[2pN \int_{-\pi/6p}^{\pi/6p} RlB\,(\alpha, t)\,d\alpha\right] \tag{7}$$

Substituting (7) in (5), the electromagnetic torque expression becomes

$$T_a\,(t) = \frac{e_a\,(t)\,i_a\,(t)}{\omega_m} \tag{8}$$

The total instantaneous electromagnetic torque is the sum of the torques produced by phases a, b, and c:

$$T_{em}\,(t) = \frac{1}{\omega_m}\left[e_a\,(t)\,i_a\,(t) + e_b\,(t)\,i_b\,(t) + e_c\,(t)\,i_c\,(t)\right] \tag{9}$$

Torque ripple factor is zero for the case of sinusoidal back EMF's and the converter-fed stator currents with the electromagnetic torque is constant. However, due to the PMSM stator construction and the step magnetic field distribution, the induced back EMF's are non-sinusoidal rich in high-order harmonics. In this case, with sinusoidal stator currents also, torque ripple will be present. If PMSM drive is supplied with non-sinusoidal current, the torque ripple will get enhance substantially. For PMSM, the torque ripple frequency will be equal to six-times the converter-fed stator feed frequency. Hence, the electromagnetic torque developed by PMSM will have an mean torque component as well as torque harmonics of order multiple of six, as given in (10):

$$T_{em} = T_0 + \sum_{n=1}^{\infty} T_{6n} \cos\left(n6\omega t + \emptyset_{6n}\right) \tag{10}$$

where T_0 is the mean electromagnetic torque and T_{6n} are harmonic torques. The Torque Ripple Factor (TRF) can be given as the peak-to-peak torque ripple values by mean electromagnetic torque developed:

$$TRF = \frac{T_{pp}}{T_0} \tag{11}$$

where T_{pp} is peak-to-peak electromagnetic torque ripple value.

Since the torque harmonics/ripples are function of stator current time-harmonics/ripples which in turn contributes to

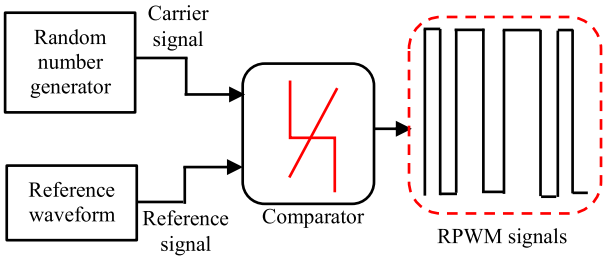

FIGURE 2. Block diagram of generation of RPWM signals in MATLAB/Simulink tool.

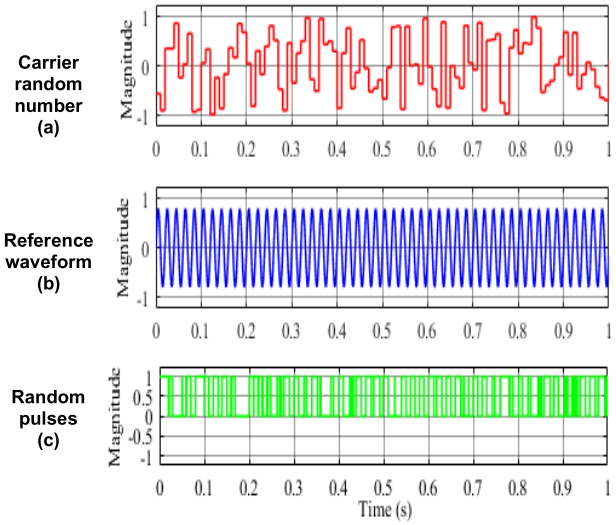

FIGURE 3. Intermediate waveforms for a generation of RPWM signals for three-phase inverter.

production of ANV in PMSM. It is possible by employing spread spectrum RPWM technique, then to spread out the frequency spectrum of the harmonic voltage, and therefore current, towards higher order in such a way as to significantly damp lower order current time harmonics magnitude for torque ripple minimization. Also, higher order stator current time harmonics may be filtered out due to PMSM stator winding inductance which will further reduce the torque ripples.

III. RANDOM PWM TECHNIQUE FOR PMSM DRIVE

If PMSM drive runs through fixed frequency PWM pulses, the noise (acoustic) generated by the drive will be higher. Therefore, in this paper, an RPWM technique i.e. random pulse position, has been proposed to utilize for minimization of the ANV in PMSM drive. The block diagram of RPWM signals generation is shown in Fig. 2. In the RPWM method, the pulses of switching signals are randomly placed in individual switching intervals. The simplest approach generally used to place randomly pulse position either at beginning or at the end of the switching interval. The randomly generated fractional numbers, n, having uniform probability distribution, are compared with the desired duty ratios of the switching signals for individual phases of the inverter.

Intermediate waveforms for a generation of RPWM signals for three-phase inverter are shown in Fig. 3. Random bit

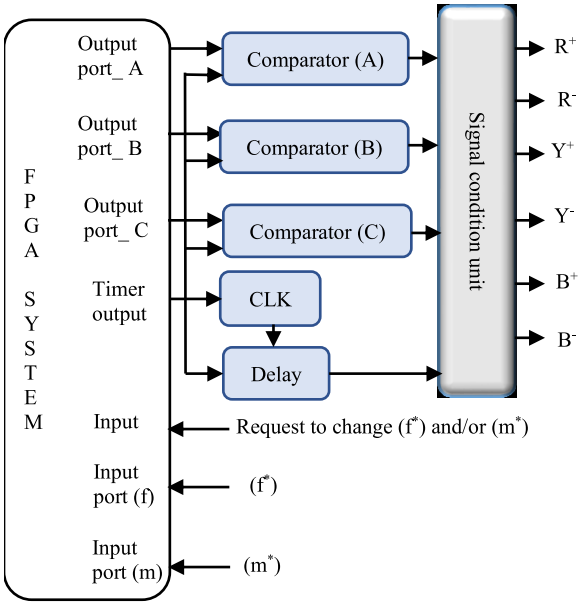

FIGURE 4. Schematic layout of an FPGA based generated RPWM signals for a three-phase inverter.

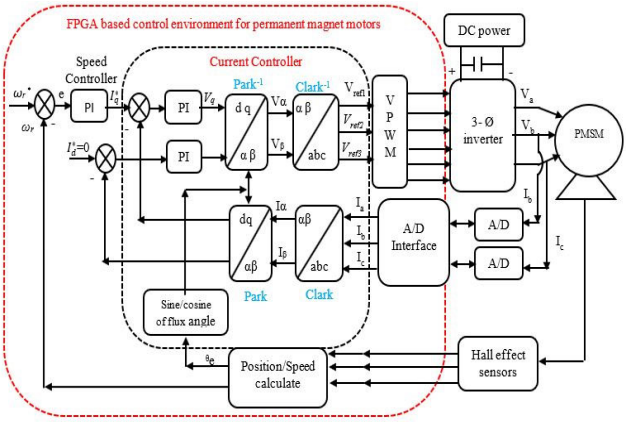

FIGURE 5. A schematic diagram of vector control based PMSM drive.

generator generates a random number as shown in Fig. 3 (a) and those random numbers compared with carrier wave as shown in Fig. 3 (b). Finally, generated RPWM signals based on a comparison between random number and carrier signals are shown in Fig. 3 (c). A schematic layout of a generation of Field Programmable Gate Array (FPGA) based RPWM signal for a three-phase inverter is shown in Fig. 4. A generated RPWM, by varying the value of the output frequency (f^*) (maximum frequency range 20 kHz) and modulation index (m^*) (the maximum modulation index is 0.8).

The FPGA based control structure of the PMSM drive is shown in Fig. 5. To control the dynamic and steady-state speed response of PMSM drive, cascaded control principle including a Proportional and Integral (PI) current controller (inner- loop) and a PI speed controller (outer-loop) has been used with a sinusoidal PWM and RPWM techniques for three-phase VSI fed PMSM drive.

The design of a PI speed controller is performed using transfer function model of PMSM drive as elaborated in [15]. The PMSM and inverter open-loop transfer function is given by (12), as shown at the bottom of this page.

The inner current loop transfer function is given in (13), as shown at the bottom of this page; where $T_a = (L_q/R_s)$, $K_m = (1/B_t)$, $T_m = (J/B_t)$ and $K_b = K_t K_m \lambda_{af}$, and $K_t = (3/2)\ (P/2)^2 \lambda_{af}$. Where P is number of rotor poles. From Fig. 6, the block diagram of a closed-loop transfer function of PMSM drive is obtained, as given in (14);

$$\frac{\omega_r(s)}{\omega_r{*}(s)} = \frac{1}{H_\omega} \frac{K_g \frac{K_s}{T_s}(1+sT_s)}{s^3 T_{\omega i} + s^2 + (1+sT_s) K_g \frac{K_s}{T_s}} \tag{14}$$

where, $K_g = ((K_i K_t K_m H_\omega)/T_m)$, $K_{in} = 0.65(V_{dc}/V_{cm})$, $T_{in} = (1/2 f_c)$, $T_s = 6T\omega_i$ and $K_i = (K_{in} T_m/K_b)$.

V_{dc} is the dc-link voltage, V_{cm} is the maximum control voltage, f_c is the switching frequency of the inverter, H_ω is damping ratio (0.707), K_t is torque constant, K_m is mechanical gain, T_m mechanical time constant. The bode plot and frequency response of speed control of PMSM drive is discussed in section V.

A brief analysis about how RPWM improves torque ripples, vibration and acoustic noise of PMSM drives is discussed as follows. Power dissipation (P_k) in the k^{th} harmonic of current, when regular PWM techniques are used. The power dissipation in the k^{th} harmonic P_k is derived by (15) [9],

$$P_k \propto \left| E\left\{ \sum\nolimits_{n=1}^{\tau} \bar{a}_n \frac{sin\left(\pi \frac{k}{\tau} \bar{a}_n\right)}{\left(\pi \frac{k}{\tau} \bar{a}_n\right)} \cdot e^{-j2\pi k/\tau n e^{-j2\pi k/\tau \theta_n}} \right\} \right|^2 \tag{15}$$

where, E $\{\cdot\}$ and $\bar{a}_n$, are a statistical expectation and duty cycle respectively where 'n' denotes n^{th} switching interval of an inverter, 0 and τ are random variables. θ_n represents the random variable position of pulses in the n^{th} interval which varies from $((a_n - 1)/2)$ to $((1- a_n)/2)$. Considering the randomization in θ_n with an equal probability interval of $\pm\ ((1- a_n)/2)$ then lead-lag RPWM power dissipation can be written by (16);

$$P_k \propto \left| \left\{ \sum\nolimits_{n=1}^{\tau} \frac{\bar{a}_n \frac{sin\left(\pi \frac{k}{\tau} \bar{a}_n\right)}{\left(\pi \frac{k}{\tau} \bar{a}_n\right)} \cdot e^{-\frac{j2\pi k}{\tau n}}}{cos\left[\pi \frac{k}{\tau}(1 - \bar{a}_n)\right]} \right\} \right|^2 \tag{16}$$

Eq. (16) shows that when θ_n, is a random variable, then each term in the series is reduced by a cosine factor. Power of the k^{th} harmonic is reduced accordingly, and the power lost is transferred to a continuous spectrum. The extent of this reducing effect depends on the k/τ ratio. The most pronounced harmonics, i.e., those near the multiples of the switching frequency, still tend to significantly exceed the level of the continuous spectrum. In a nutshell, the randomization of the pulse position acuminate the frequency spectrum by reducing most harmonics below the level of the continuous spectrum and leaving narrow clusters of harmonics in the vicinity of multiples of the switching frequency [9].

IV. NON-LINEAR ELECTRODYNAMIC MODELING OF PMSM DRIVE

The relation of total flux and forces with the current has been proposed as non-linear in terms of electrodynamic behavior of PMSM drive [1]. Magnitude of the exciting electromagnetic forces and harmonic forces vicinity to any modal frequency are primarily the causes of electromagnetic vibration and noise emissions from the electric machines. Frequencies corresponding to the peak values are the resonance frequencies and are also known as modal frequencies. In addition, the understanding of forces harmonic spectrum takes into account both the factors that are magnitude and proximity of harmonic forces. However, the resultant force will be having the dominance of all the radial forces depending upon the combination of aforementioned factors. Therefore, in this work, the calculation of the dominant radial forces is vital, to calculate acoustic noise, vibrations and torque ripples.

Measurement of acoustic noise and vibrations are very much different rather calculating. Several Finite Element (FE) software's like ANSYS, etc. offer leading software simulation packages for this purpose. Using the Finite Element model, it is possible to calculate accurately the acoustic noise and vibrations originated by any given set of radial and tangential forces. The magnitude of the vibration for calculating acoustic noise is generally turned out to be the resultant of all external surfaces of electric machine vibrations. Finite Element model is commonly used to find a point wise approximation in the form of a single source of noise. However, the radiation efficiency used for calculating acoustic noise strongly depends on the dimension and the shape of the noise source [16].

The stator system, that is, the stator core, winding, and frame (enclosure) is considered as a single thick ring loaded with teeth and winding. The natural frequency (f_m) of the stator system of the m^{th} circumferential vibrational mode can be expressed by (17) [1]:

$$f_m = \frac{1}{2\pi} \sqrt{\frac{K_m}{M_m}} \tag{17}$$

where K_m is the lumped stiffness (N/m) and M_m is the lumped mass (kg) of the stator system. The amplitude of vibration

$$G = \frac{\omega(s)}{I_q(s)} = \frac{K_{in} K_t}{(1+sT_m)\left(R_s + sL_q\right)(B_t + sJ) + K_{in}(B_t + sJ) + K_t \lambda_a (1+sT_m)} \tag{12}$$

$$\frac{i^r_{qs}(s)}{i^r_{qs}{*}(s)} = \frac{K_{in} K_t (1+sT_m)}{H_c K_a K_{in}(1+sT_m) + (1+sT_{in})\{K_a K_b + (1+sT_a)(1+sT_m)\}} \tag{13}$$

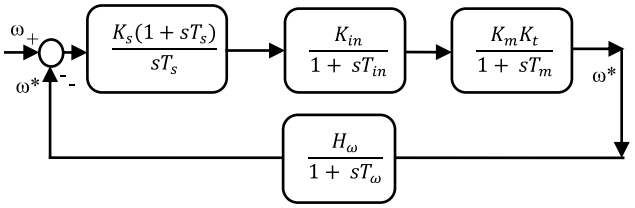

FIGURE 6. Block diagram of simplified speed loop of PMSM drive.

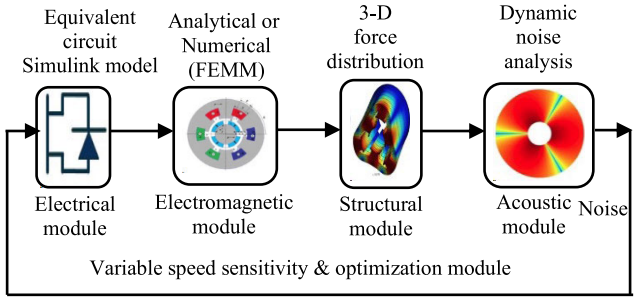

FIGURE 7. Pictorial view of the MANATEE simulation process.

displacements of mode m can be derived as (18) which require development of FE models for calculations.

$$A_m = \frac{F_m/M}{\sqrt{\left(\omega_m^2 - \omega_r^2\right)^2 + 4\xi_m^2\omega_m^2\omega_r^2}} \tag{18}$$

here M is the mass (kg) of the cylindrical shell, ω_m is the angular natural frequency of the mode m, $\omega_{\rm r}$ is the angular frequency of the force component of the order r, and $\xi_{\rm m}$ is the modal damping ratio. The amplitude of force $F_{\rm m} = \pi D_{1{\rm in}} L_{\rm i} P_{\rm mr}$, in which D_{1in} is the inner diameter of the stator core, L_i is the effective length of the stator core, and P_{mr} is the magnitude of the magnetic pressure of the order r [1].

A general expression for the modal radiation efficiency of finite length cylindrical frame defined by (19);

$$\sigma_{mn(\omega)} = \frac{\pi_{mn(\omega)}}{\rho_0 c_0 S\left(\bar{v_{mn}^2}\right)} \tag{19}$$

where, m is a circumferential mode, n is axial mode, ρ_0 is air density at $20°C$, c_0 is sound speed in the air at 1000 mbar, S is a surface area in m^2, v is a linear velocity which require FE models for calculations based on exact rotor speed and force at a given time instant.

The radiated acoustic power can be defined by (20);

$$\pi \approx \pi_m = \rho_0 c_0 \left(\frac{\omega A_m}{\sqrt{2}}\right)^2 \sigma_m S_f \tag{20}$$

The sound power level can be expressed by (21)

$$L_w = 10\log_{10}\frac{\pi}{\pi_{ref}} \tag{21}$$

The reference sound power $\pi_{\rm ref} = 10^{-12}$ W is corresponding to the refence sound intensity transmitted through a unit area.

In this paper, the simulation studies have been performed using MATLAB/Simulink and Magnetic Acoustic Noise Analysis Tool for Electrical Engineering (MANATEE) software [17]. The analysis of vibration and acoustic noise of PMSM drive is not feasible in MATLAB/Simulink software. Analysis of acoustic noise of PMSM drive has been simulated in MANATEE. Fig. 7 shows the MANATEE simulation flow which contains four modules such as Electrical, Electromagnetic, Structural and Acoustic module.

The most important and useful fluxes are radial and tangential fluxes to analyze the ANV of PMSM drive. The radial and tangential fluxes are the main sources of generation of ANV in PMSM drive. Simulation results obtained from MANTEE simulation process of the acoustic noise of the PMSM drive are shown in Fig. 8. The time-domain and the frequency-domain response of airgap radial flux density and tangential flux density at $\alpha_{\rm s} = 0°$ as a function of time is shown in Fig. 8 (a). The 3-D plot of airgap radial flux density as a function of time and space is shown in Fig. 8 (b). In order to analyze the machine acoustic behavior; computed noise power level spectrum at variable speed, along with a sonogram is shown in Fig. 8 (c).

Results clearly identify the magnitude of flux density of permanent magnet and types of the force responsible i.e. radial forces for the production of ANV in PMSM drive. The sound power spectrogram gives maximum sound level generates at different inverter switching frequency and operational speed. Hence, the concerned inverter switching frequency may be avoided by implementing suitable control algorithms for the reduction of ANV in the PMSM drive.

V. SIMULATION AND EXPERIMENTAL INVESTIGATIONS

The experimental results are obtained on a 1.07 kW small-scaled laboratory setup to validate the effectiveness of the proposed RPWM scheme. The parameters and system configurations are given in Table-1 and Figs. 9 and 10, respectively. A low-cost acoustic chamber has been developed in laboratory to investigate the ANV from PMSM drive. The pictorial view of a low-cost acoustic chamber with the sensors and PMSM is shown in Fig. 11. For simulation studies, MATLAB/Simulink tool is employed. In experimental set-up, PMSM is coupled with DC shunt motor and fed from Semikron converter. Data Acquisition (DAQ) system for ANV measurement is from National Instrument (NI).

A. SIMULATION RESULTS OF SPWM AND RPWM TECHNIQUES FOR PMSM DRIVE

The SPWM technique is implemented to observe and analyze speed response, torque ripple and stator current of PMSM drive. Further RPWM technique is implemented for the reduction of torque ripple and ANV of PMSM drive. The analysis of the ANV of PMSM drive is not possible in the MATLAB/Simulink platform because of the limitation

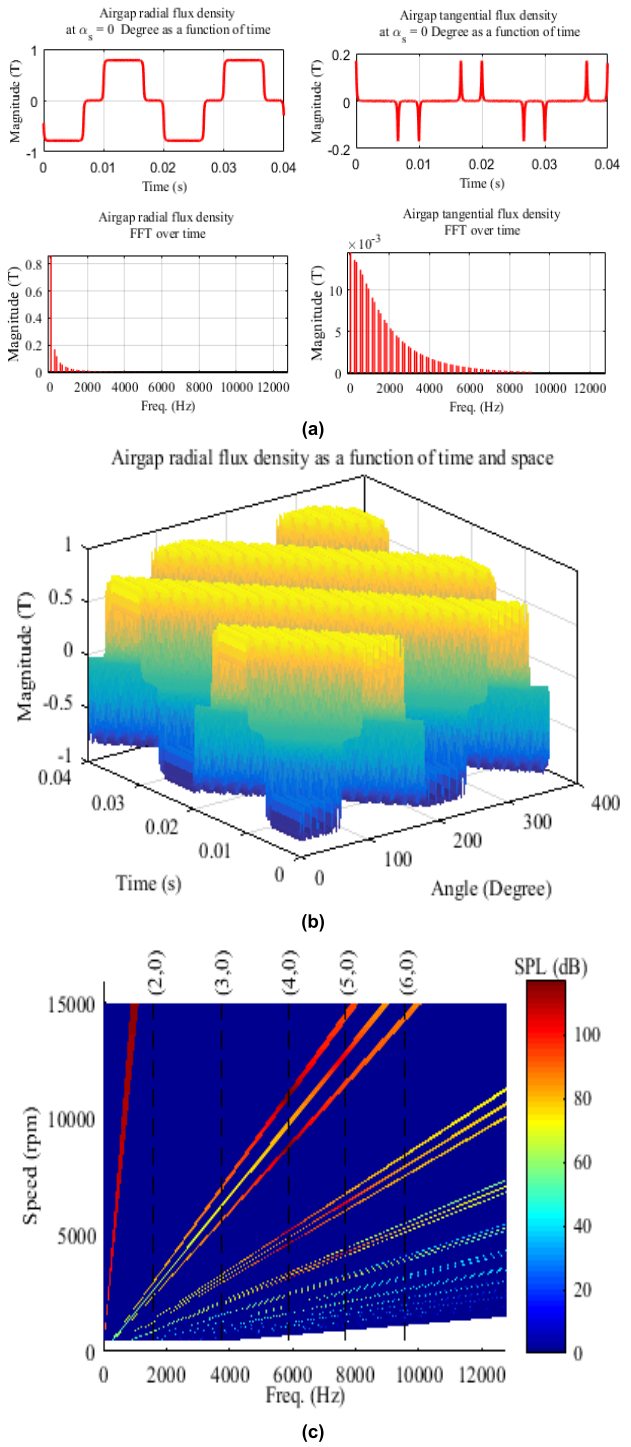

FIGURE 8. Simulation results of acoustic noise of PMSM drive: (a) time and frequency domain response of airgap radial flux density and tangential flux density at $\alpha_s = 0°$ as a function of time, (b) airgap radial flux density as a function of time and space and (c) sound power spectrogram of PMSM drive.

TABLE 1. Experimental set-up specification.

Specification Item	Value	Unit
PMSM Rated Power	1.07	kW
PMSM Rated speed	3000	rpm
No. of poles	04	
Torque constant stall	3.6	N-m
Current constant stall	6.29	A
Rated DC bus voltage	300	V
PMSM per phase Resistance	3.07	ohm
PMSM per phase Inductance	6.57	mH
Linkage flux	0.1546	Wb-turn
Rotor inertia	1.4-1.8	kg-m^2
Spartan 3AN FPGA kit	20	MHz clock frequency
PMSM Peak current	16	A
IGBT (instantons voltage and current)	600, 30	V, A
Accelerometer sensitivity (PCB Piezotronics 352C03)	10	mV/g
Microphone (half-inch free field) (National Instrument USB 4432)	10	mV/Pa

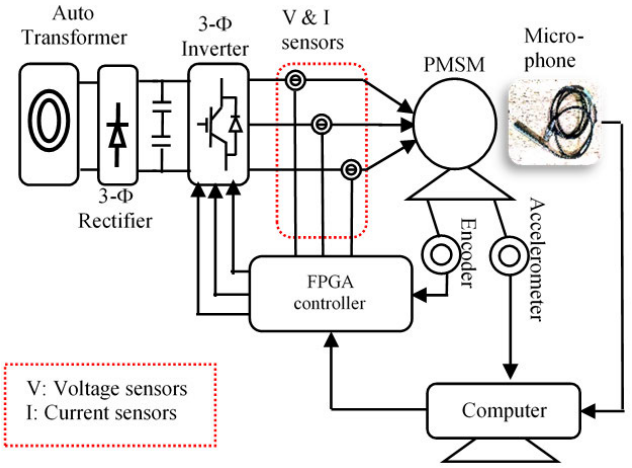

FIGURE 9. Schematic diagram of experimental setup.

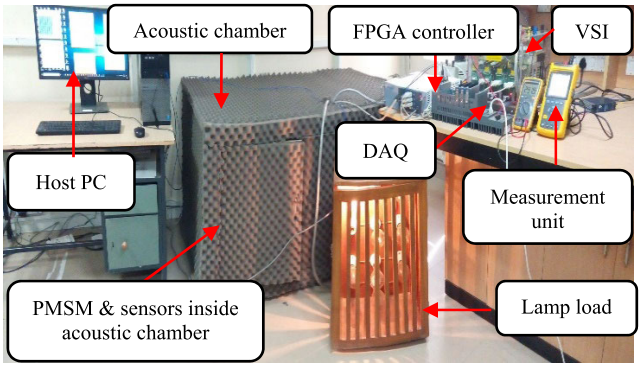

FIGURE 10. An experimental setup for analysis of ANV of PMSM drive.

of the software itself. Henceforth, the analysis is primarily focused on comparison of torque ripple of PMSM drive for different control strategy as magnitude of ANV is related to torque ripple.

Simulations are carried out for drive speed of 1000 rpm and mechanical loading T_m of 1 N-m and results are shown in Fig. 12. Three-phase stator line-line voltage V_{ab}, V_{bc} and

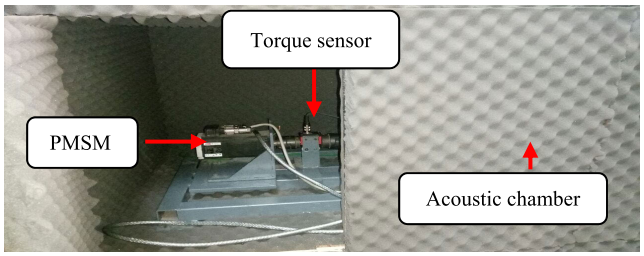

FIGURE 11. Acoustic chamber with sensors and PMSM drive.

TABLE 2. Comparison of torque ripples of PMSM drive for SPWM and RPWM techniques.

Parameters	SPWM	RPWM
$T_{max.}$ (N-m)	2.309	1.571
$T_{min.}$ (N-m)	0.1853	1
$T_{avg.}$ (N-m)	1.247	1.285
T_{ripple} (N-m)	1.70	0.44

V_{ca} of PMSM drive are shown in Fig. 12 (a). Each phase is 120° shifted with respect to each other. DC link reference is set at 300 V. Non-sinusoidal stator current of converter-fed PMSM drive is shown in Fig. 12(b).

The α-β axis magnetic flux response of PMSM drive is shown in Fig. 12 (c). The Total Harmonic Distortion (THD) of magnetic flux waveform is 43.25% and 28.63% for SPWM and RPWM, respectively.

RPWM is implemented as discussed in previous section and generated RPWM signal for switching operation of inverter is shown in Fig. 12 (d). In RPWM, the pulses of switching signals are randomly placed in individual switching intervals. Due to RPWM signals, the stator voltage and in-turn stator current harmonic spectrum gets spread out and distributed towards the higher order of harmonics. The THD of stator current reduces from 46.73% for SPWM to 33.58% for RPWM technique.

The steady-state speed response of the PMSM drive is shown in Fig. 12 (e) for a reference speed of 1000 rpm. The speed controller guided the PMSM drive to follow set reference speed. The settling time for speed response for RPWM is around 0.02 s. Shorter settling time of a speed response is key characteristics of a high-performance PMSM drive.

Torque response for RPWM technique exhibits excellent performance with almost one-fourth reduction in torque ripples as compared to SPWM technique, as shown in Fig. 12 (f). Reduction in torque ripple response is evidently related with reduction in stator current harmonics. Torque ripples reduction will in turn leads to reduction in vibration and acoustic noise. Table-2 presents quantitative comparative results for torque profile of PMSM drive.

Furthermore, simulations are carried out for dynamic speed response and torque performance with mechanical loading T_m of 1 N-m and results are shown in Fig. 13 (a) and (b), respectively. The speed of the PMSM drive varied dynamically from 0 to 1 s. The dynamic speed of the PMSM drive from 0 to 0.2 s is 600 rpm, 0.2 to 0.5 s 1500 rpm and 0.5 to 1 s

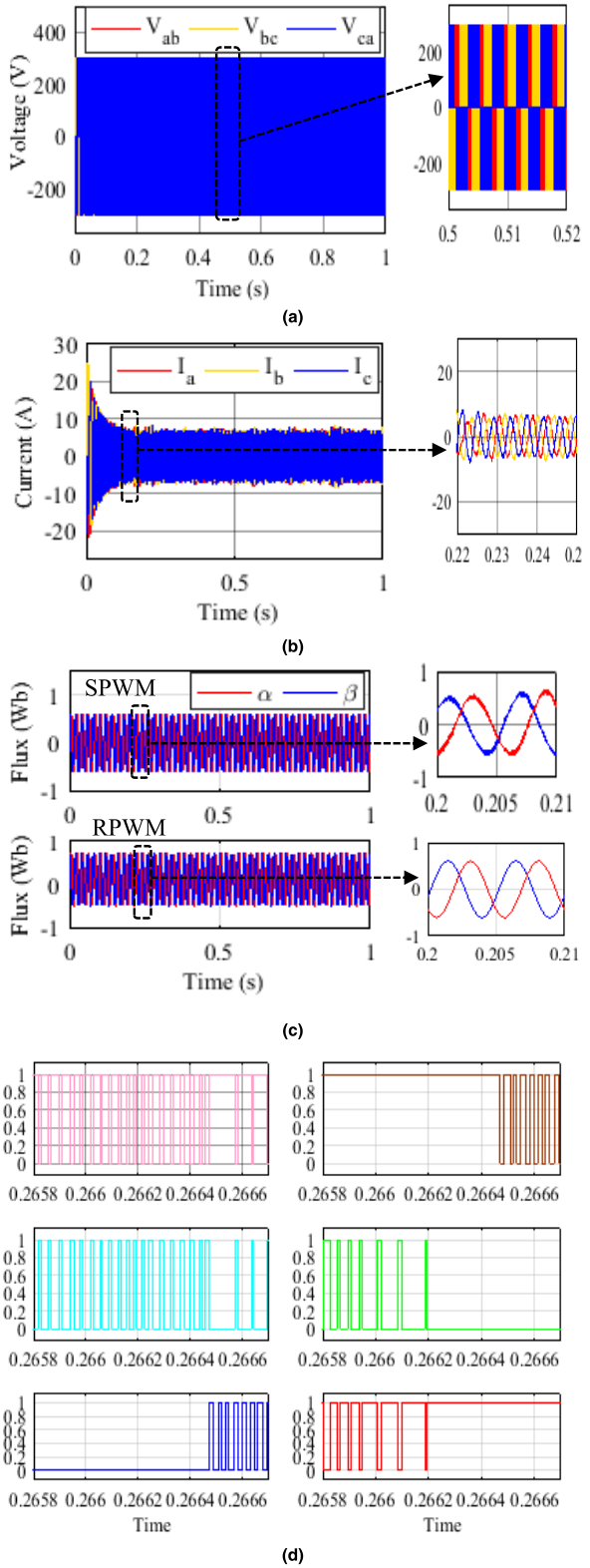

FIGURE 12. Simulation results of PMSM drive: (a). Three-phase stator voltage response, (b) three-phase stator current response, (c) α-β axis magnetic flux response, (d) RPWM signal for three-phase inverter, (e) steady-state speed response, and (f) steady-state torque response.

400 rpm. The dynamics of speed response is comparable for both techniques. However, RPWM performs better in terms of well-behaved response with less torque ripple.

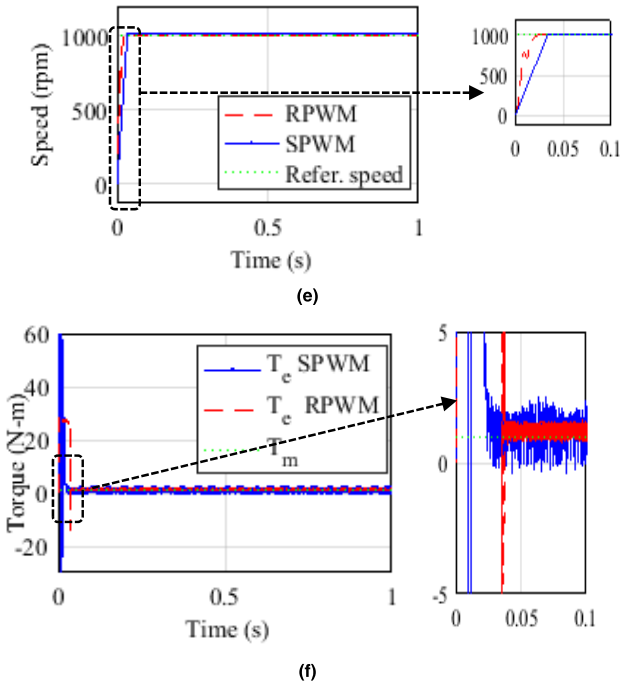

FIGURE 12. *(Continued.)* **Simulation results of PMSM drive: (a). Three-phase stator voltage response, (b) three-phase stator current response, (c) α-β axis magnetic flux response, (d) RPWM signal for three-phase inverter, (e) steady-state speed response, and (f) steady-state torque response.**

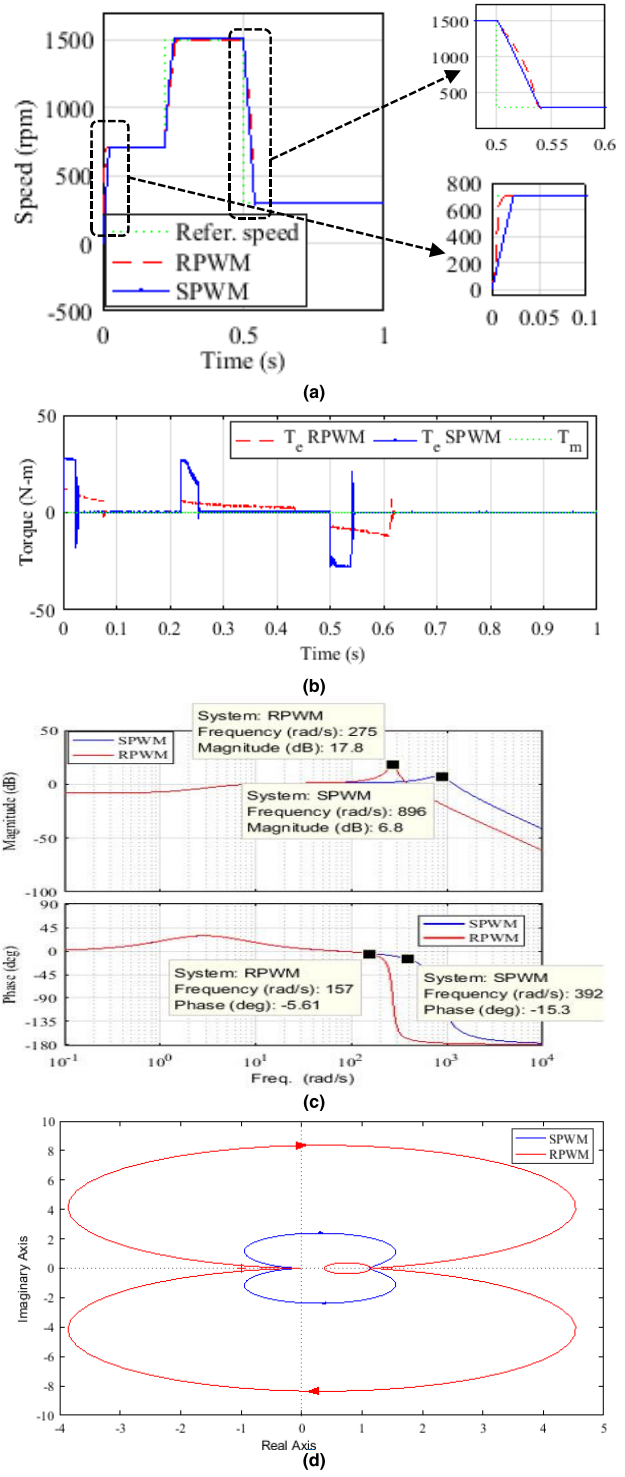

FIGURE 13. **Simulation results of PMSM drive: (a) dynamic speed response, (b) dynamic torque response, (c) frequency response of PMSM drive and (d) Nyquist response.**

Fig. 13 (c) shows a frequency response of the transfer function model of PMSM drive. The magnitude and phase plots show that the speed gain for RPWM and SPWM technique is 17.8 dB and 6.8 dB at 275 rad/s and 896 rad/s, respectively. The system has the phase of -5.6° at 157 rad/s for the RPWM technique and the phase of -15.3° at 392 rad/s for the SPWM technique. Hence, it is found that the RPWM technique for PMSM drive is highly stable with enough phase margin at the required cross over frequency.

Fig. 13 (d) shows a Nyquist response of the PMSM drive. In cartesian coordinates, the real part of the transfer function is plotted on the X-axis, and the imaginary part is plotted on the Y-axis. The frequency is swept as a parameter, resulting in a plot based on frequency.

B. EXPERIMENTAL RESULTS OF SPWM AND RPWM TECHNIQUES FOR PMSM DRIVES

Experimental results for operation of PMSM drive for SPWM and RPWM techniques are shown in Figs. 14 to 17. The three-phase stator voltages and currents of the PMSM drive are shown in Figs. 14 (a)-(b). Three-phase stator current is sinusoidal with amplitude of 2 A and 120° phase shift. Experiments are carried out for reference drive speed of 1000 rpm and mechanical loading T_m of 1 N-m. The steady-state speed response of SPWM and RPWM technique based PMSM drive is shown in Fig. 14 (c). The RWPM performs better in terms of speed response as the settling time for RPWM is 0.01s and SPWM is 0.07s.

Fig. 14 (d) shows electromagnetic torque response of the PMSM drive. The electromagnetic torque ripple for

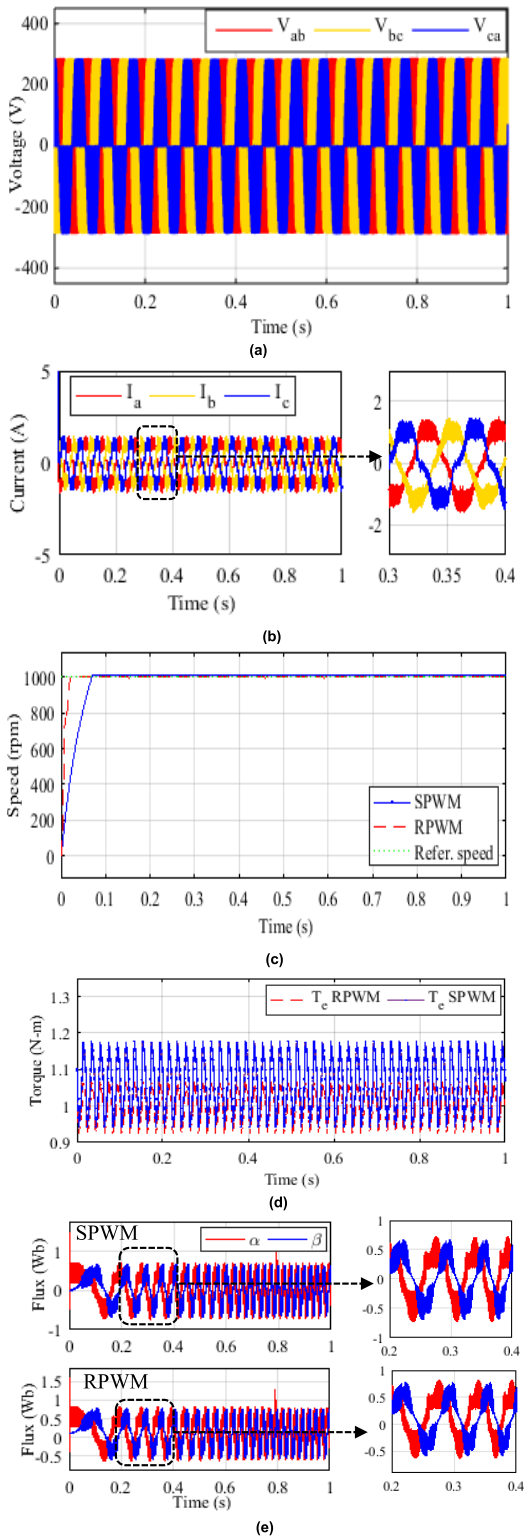

FIGURE 14. An experimental result of PMSM drive: (a) Three-phase stator voltage response, (b) three-phase stator current response, (c) steady-state speed response (reference speed 1500 rpm), (d) torque response and (e) α-β axis magnetic flux response.

SPWM and RPWM technique is calculated as 0.209 N-m and 0.128N-m, respectively. Reduction in torque ripple values clearly indicate that RPWM operated PMSM drives may have substantial reduction of vibration and acoustic noise as compared to the SPWM technique. The α-β axis magnetic flux response of PMSM drive is shown in Fig. 14 (e).

TABLE 3. Comparison of torque ripples of PMSM drive for SPWM and RPWM techniques.

Parameters	SPWM	RPWM
$T_{max.}$ (N-m)	1.177	1.072
$T_{min.}$ (N-m)	0.9547	0.943
$T_{avg.}$ (N-m)	1.0658	1.0075
T_{ripple} (N-m)	0.209	0.128

Table-3 presents numeric comparative experimental results for torque ripple of PMSM drive.

Fig. 15 show the experimental result of ANV using SPWM and the RPWM technique operated in the PMSM drive. The output sensitivity of the microphone is 10 *mV/Pa* which is situated in alignment with the radial axis of one of the stator poles. As per ISO standards, the microphone is placed 5 *cm* far away from the shaft of the PMSM [18], also a half-inch free-field microphone is to measure the acoustic noise.

The time and frequency domain sound spectrum of PMSM drive for its operation from SPWM and RPWM techniques are shown in Figs. 15 (a)-(b), respectively. Sound spectrum of PMSM drive measured in a free-field environment i.e. inside the acoustic chamber. The maximum amplitude of the sound spectrum is coming out around 1.67 *Pa* and 1.12 *Pa*, respectively observed at 14.5 *Hz* which clearly show that acoustic noise from SPWM is high as compared to the RPWM technique. Hence justifying the application of the RPWM technique for PMSM drives.

The time and frequency domain vibration spectrum of sinusoidal carrier-based PWM and RPWM techniques based PMSM drive is shown in Figs. 16 (a)-(b), respectively. Accelerometer sensor is deployed horizontally on end body of PMSM drive to measure vibration. Accelerometer sensor, having an output sensitivity of 10 *mV/g*, is attached with help of beeswax behind stator pole in order to measure vibration from the motor. The sampling rate of the sound and vibration data recorded through DAQ is 50000.

The maximum amplitude of the vibration spectrum is observed around 1.4 and 0.8 gravitation for SPWM and RPWM, respectively, with the reference set-speed of 1000 rpm. That means vibration in SPWM is almost double as compare to the RPWM technique, as shown in Fig. 16.

The harmonic frequency spectrum and Total Harmonic Distortion (THD) of PMSM stator current for SPWM and RPWM techniques are shown in Fig. 17. THDs are 60.86 % and 51.04 % for SPWM and RPWM, respectively. The harmonic analysis clearly indicates the superiority of RPWM for the reduction of ANV in the PMSM drive.

Table-4 shows the comparison of the experimentally measured acoustic noise of the PMSM drive with SPWM and RPWM techniques. For applied load torque of 1 N-m, the

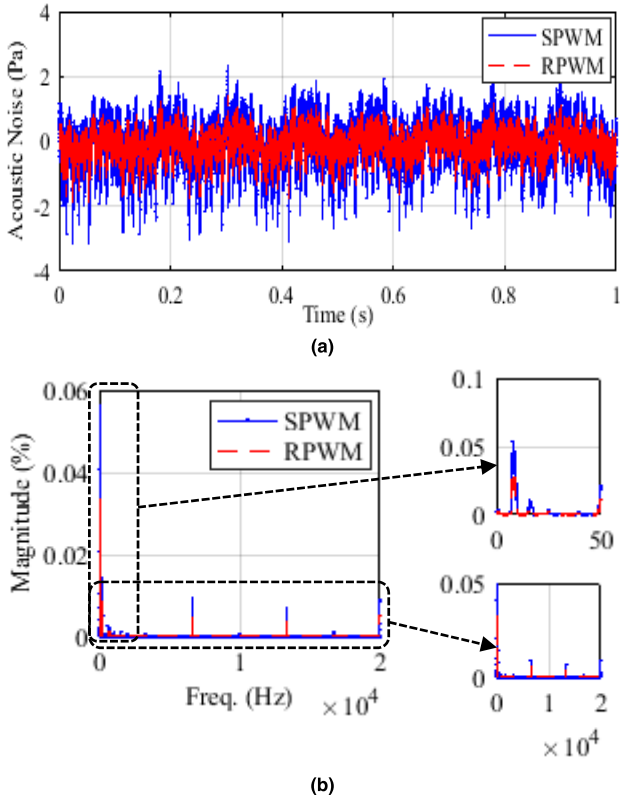

FIGURE 15. An experimental result of time and frequency domain sound spectrum of PMSM drive.

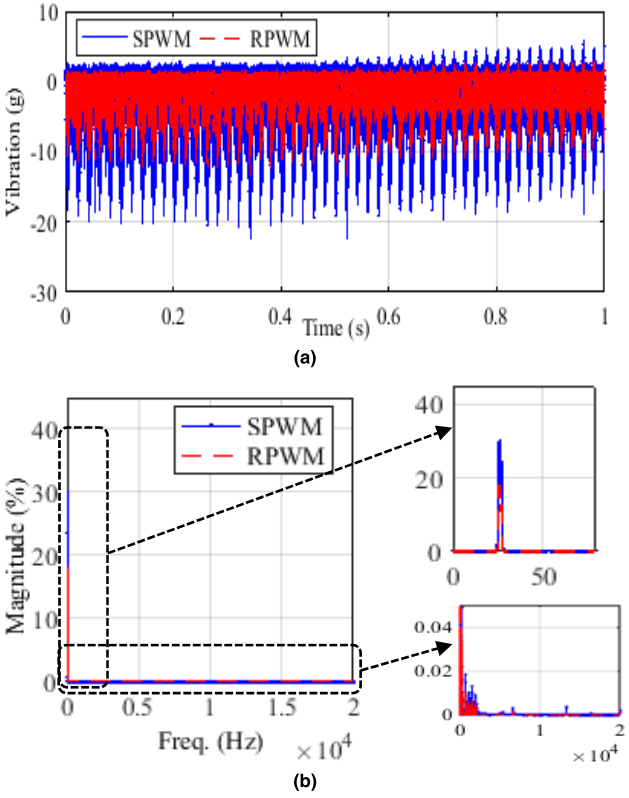

FIGURE 16. An experimental result of time and frequency domain vibration spectrum of PMSM drive.

TABLE 4. Comparison of acoustic noise of PMSM drive.

Sr. No.	T_m (N-m)	Acoustic noise (Pa)		acoustic noise reduction (%)
		With SPWM	With RPWM	
1	1	1.8	0.9	50
2	1.5	2.3	1.6	30.43
3	2	2.5	1.9	26.08

TABLE 5. Comparison of vibration of PMSM drive.

Sr. No.	T_m (N-m)	Vibration (g)		Vibration reduction (%)
		With SPWM	With RPWM	
1	1	1.4	0.8	42.85
2	1.5	2.2	1.4	36.36
3	2	2.7	1.8	33.33

significant amount of noise reduction can be seen for the RPWM technique, which is nearly 50% less, as compared to SPWM. Similarly, Table-5 shows the values of vibration in *g* of PMSM drive. There is reduction of vibration of the order of 40% in the case of RPWM technique as compared to SPWM.

RPWM technique proves to be effective for the substantial reduction of torque ripples and in-turn acoustic noise and vibration in the PMSM drive. However, RPWM may pose few limitations such as challenges in device loss calculation, thermal and loop control design and hence thermal subsystems cannot be optimally designed.

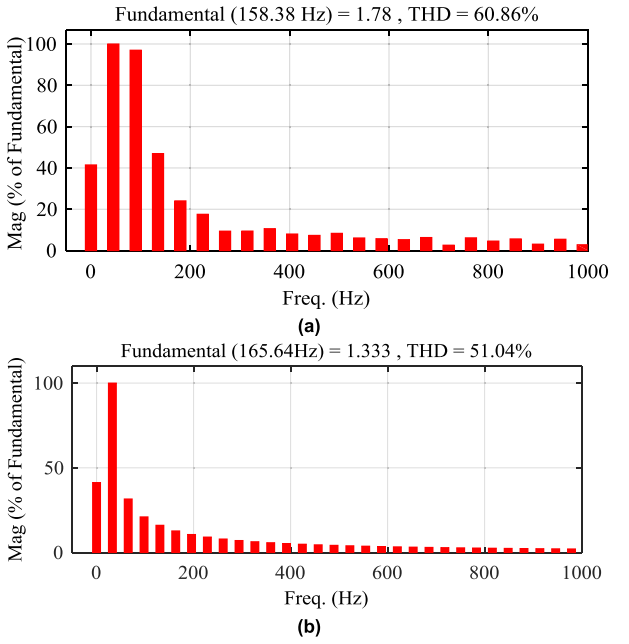

FIGURE 17. Experimental results of PMSM drive: (a) stator current harmonic with SPWM and (b) RPWM technique.

VI. CONCLUSIONS

This paper has presented a novel application of the harmonic spread spectrum technique, that is, Random Pulse Width Modulation (RPWM) in order to reduce Acoustic Noise and Vibration (ANV) in the Permanent Magnet Synchronous

Motor (PMSM) drives. RPWM is a spread spectrum technique that spreads the acoustic noise frequency spectrum over a wide range in contrast to the sinusoidal PWM, which is concentrated at particular frequencies. With the result, the overall effect of noise is significantly reduced. Experimental results, obtained on a small-scale laboratory set-up, have confirmed substantial reduction of ANV of the order of 40% and the torque ripple around 35% by the application of RPWM technique in comparison with the conventional sinusoidal PWM technique.

REFERENCES

[1] J. F. Gieras, C. Wang, and J. C. S. Lai, *Noise of Polyphase Electrical Motors*. New York, NY, USA: Taylor & Francis, 2006.
[2] I. P. Tsoumas and H. Tischmacher, "Influence of the Inverter's modulation technique on the audible noise of electric motors," *IEEE Trans. Ind. Appl.*, vol. 50, no. 1, pp. 269–278, Jan. 2014.
[3] A. Andersson, D. Lennstrom, and A. Nykanen, "Influence of inverter modulation strategy on electric drive efficiency and perceived sound quality," *IEEE Trans. Transport. Electrific.*, vol. 2, no. 1, pp. 24–35, Mar. 2016.
[4] A. C. Binojkumar, B. Saritha, and G. Narayanan, "Acoustic noise characterization of space-vector modulated induction motor Drives—An experimental approach," *IEEE Trans. Ind. Electron.*, vol. 62, no. 6, pp. 3362–3371, Jun. 2015.
[5] Y. Fang and T. Zhang, "Sound quality of the acoustic noise radiated by PWM-fed electric powertrain," *IEEE Trans. Ind. Electron.*, vol. 65, no. 6, pp. 4534–4541, Jun. 2018.
[6] Z. Q. Zhu, Z. P. Xia, L. J. Wu, and G. W. Jewell, "Influence of slot and pole number combination on radial force and vibration modes in fractional slot PM brushless machines having single- and double-layer windings," in *Proc. IEEE Energy Convers. Congr. Exposit.*, Sep. 2009, pp. 3443–3450.
[7] H.-Y. Yang, Y.-C. Lim, and H.-C. Kim, "Acoustic noise/vibration reduction of a single-phase SRM using skewed stator and rotor," *IEEE Trans. Ind. Electron.*, vol. 60, no. 10, pp. 4292–4300, Oct. 2013.
[8] J.-W. Jung, S.-H. Lee, G.-H. Lee, J.-P. Hong, D.-H. Lee, and K.-N. Kim, "Reduction design of vibration and noise in IPMSM type integrated starter and generator for HEV," *IEEE Trans. Magn.*, vol. 46, no. 6, pp. 2454–2457, Jun. 2010.
[9] A. M. Trzynadlowski, F. Blaabjerg, J. K. Pedersen, R. L. Kirlin, and S. Legowski, "Random pulse width modulation techniques for converter-fed drive systems—A review," *IEEE Trans. Ind. Appl.*, vol. 30, no. 5, pp. 1166–1175, Oct. 1994.
[10] W. Zhang, Y. Xu, H. Huang, and J. Zou, "Vibration reduction for dual-branch three-phase permanent magnet synchronous motor with carrier phase-shift technique," *IEEE Trans. Power Electron.*, vol. 35, no. 1, pp. 607–618, Jan. 2020.
[11] J. Zou, H. Lan, Y. Xu, and B. Zhao, "Analysis of global and local force harmonics and their effects on vibration in permanent magnet synchronous machines," *IEEE Trans. Energy Convers.*, vol. 32, no. 4, pp. 1523–1532, Dec. 2017.
[12] K. Basu, J. Prasad, and G. Narayanan, "Minimization of torque ripple in PWM AC drives," *IEEE Trans. Ind. Electron.*, vol. 56, no. 2, pp. 553–558, Feb. 2009.
[13] R. M. Pindoriya, G. Gautam, and B. S. Rajpurohit, "A novel application of pseudorandom based technique for acoustic noise and vibration reduction of PMSM drive," in *Proc. IEEE Ind. Appl. Soc. Annu. Meeting*, Baltimore, MD, USA, Sep. 2019, pp. 1–8.
[14] H. Le-Huy, R. Perret, and R. Feuillet, "Minimization of torque ripple in brushless DC motor drives," *IEEE Trans. Ind. Appl.*, vols. IA–22, no. 4, pp. 748–755, Jul. 1986.
[15] R. Krishnan, *Permanent Magnet Synchronous and Brushless DC Motor Drives*. Boca Raton, FL, USA: CRC Press, 2010.
[16] D. Torregrossa, A. Khoobroo, and B. Fahimi, "Prediction of acoustic noise and torque pulsation in PM synchronous machines with static eccentricity and partial demagnetization using field reconstruction method," *IEEE Trans. Ind. Electron.*, vol. 59, no. 2, pp. 934–944, Feb. 2012.
[17] *Software Manuals: The Magnetic Acoustic Noise Analysis Tool for Electrical Engineering (MANATEE)*, EOMYS Eng., France, Mar. 2019.
[18] *Reference Standards for Vibration Monitoring and Analysis*, ISO Standard 79192-2:2001, International Organization for Standardization, Geneva, Switzerland, 2001, pp. 1–10.

RAJESH M. PINDORIYA (Graduate Student Member, IEEE) received the B.Tech. degree in electrical and electronics engineering from Rajasthan Technical University Kota, India, in 2012, and the M.E. degree in power electronics and electrical drives from Gujarat Technological University, Ahmedabad, India, in 2014. He is currently a Ph.D. Researcher with the IIT Mandi, India, with a focus on design and implementation of high-performance permanent magnet synchronous motor drive.

His research interests include design controllers for the permanent magnet synchronous motor (PMSM) and brushless direct current (BLDC) motor drives. He is also working on analysis and reduction of acoustic noise and vibration of PMSM and BLDC motor drives. He is an Associate Member of the Institution of Electronics and Telecommunication Engineers (IETE) (AM'17) and the Institution of Engineering (IE) (AM'17) and a Student Member of the Industry of Electrical and Technology (IET) (STM'17).

BHARAT SINGH RAJPUROHIT (Senior Member, IEEE) received the M.Tech. degree in power apparatus and electric drives from the IIT Roorkee, Roorkee, India, in 2005, and the Ph.D. degree in electrical engineering from the IIT Kanpur, Kanpur, India, in 2010. He is currently an Associate Professor with the School of Computing and Electrical Engineering, IIT Mandi, Mandi, India. His major research interests include electric drives, renewable energy integration, and intelligent and energy-efficient buildings. He is a Senior Member of the Institution of Engineers (India).

RAJEEV KUMAR (Senior Member, IEEE) received the Ph.D. degree in machine design from the IIT Roorkee, Roorkee, India, in 2008. He is currently an Associate Professor with the School of Engineering, IIT Mandi, Mandi, India. He has given his services to the General Electric John F. Welch Technology Centre, Bengaluru, India, as a Technologist, from 2008 to 2010. His major research interests include machine design, solid mechanics, vibration, smart material/structure, piezoelectric energy harvesting, finite element method, modeling and control, and optimization (genetic algorithm).